

# Light cone dynamics and reverse Kibble-Zurek mechanism in two-dimensional superfluids following a quantum quench

L. Mathey<sup>1</sup> and A. Polkovnikov<sup>2</sup><sup>1</sup>*Joint Quantum Institute, National Institute of Standards and Technology and University of Maryland, Gaithersburg, Maryland 20899 USA*<sup>2</sup>*Department of Physics, Boston University, 590 Commonwealth Ave., Boston, Massachusetts 02215 USA*

(Received 31 December 2009; published 11 March 2010)

We study the dynamics of the relative phase of a bilayer of two-dimensional superfluids after the two superfluids have been decoupled. We find that on short time scales the relative phase shows “light cone”-like dynamics and creates a metastable superfluid state, which can be supercritical. We also demonstrate similar light cone dynamics for the transverse field Ising model. On longer time scales the supercritical state relaxes to a disordered state due to dynamical vortex unbinding. This scenario of dynamically suppressed vortex proliferation constitutes a *reverse-Kibble-Zurek effect*. We study this effect both numerically using truncated Wigner approximation and analytically within a newly suggested time dependent renormalization group approach (RG). In particular, within RG we show that there are two possible fixed points for the real-time evolution corresponding to the superfluid and normal steady states. So depending on the initial conditions and the microscopic parameters of the Hamiltonian the system undergoes a nonequilibrium phase transition of the Kosterlitz-Thouless type. The time scales for the vortex unbinding near the critical point are exponentially divergent, similar to the equilibrium case.

DOI: [10.1103/PhysRevA.81.033605](https://doi.org/10.1103/PhysRevA.81.033605)

PACS number(s): 03.75.Hh, 03.75.Mn, 05.30.Jp

## I. INTRODUCTION

The technological advances of trapping and manipulating ultracold atom systems provide an opportunity to study many-body dynamics with unprecedented clarity. The realization of Bose-Einstein condensates (BEC) in ultracold atom systems [1], the Mott insulator transition [2], the BEC-BCS transition [3], and the Kosterlitz-Thouless transition [4–6] demonstrated that this technology can be used as a quantum simulator of many-body phases. Here, the static state of a system in equilibrium is created and studied. Various dynamical aspects of ultracold atom systems were also probed, such as dipole oscillations [7], vortex excitations [8], and soliton dynamics [9], absence of equilibration in one-dimensional bosonic systems [10], spontaneous formation of vortices in spinor condensates [11], and many others (see Ref. [12] for a recent review). In Ref. [13], vortices excitations were created via laser stirring. In these experiments, the dynamics of only a few degrees of freedom were studied, such as the center-of-mass motion, or the dynamical evolution of a vortex. These experimental developments stimulated a considerable theoretical interest in understanding nonequilibrium quantum dynamics including the analysis of dynamics following sudden quenches [14], studying connections between dynamics and thermodynamics [15], and dynamics through quantum critical points [16].

The focus of this article is a detailed analysis of the full many-body dynamics following the quench in a two-dimensional quantum rotor model. Physically we imagine the situation where two initially strongly coupled superfluids are suddenly separated and we are interested in the evolution of the relative phase between the two superfluids. In particular, we will be interested in the question of how the system relaxes to the equilibrium state. We note that experiments in a similar setup involving separation of two one-dimensional (1D) superfluids were reported in Ref. [17] and the corresponding theoretical analysis was done in Refs. [18–20]. Unlike the two-dimensional (2D) case, phonon fluctuations in 1D result

in the exponential decay of the correlation functions and nonlinear effects in the form of phase slips do not bring qualitative changes to the behavior of the correlation functions at least at low initial temperatures [19].

In equilibrium for the uncoupled layers, there are two possible phases. At low temperatures atoms in each layer (which we regard as identical) form a (quasi)superfluid phase while at high temperatures they form a normal Bose gas. These phases can be distinguished by the long-range behavior of the single particle correlation function  $G(\mathbf{x}) = \langle b^\dagger(0)b(\mathbf{x}) \rangle \approx \rho \langle \exp\{i[\phi(\mathbf{x}) - \phi(0)]\} \rangle$ , where  $b(\mathbf{x})$  is the single particle operator,  $\rho$  is the atom density, and  $\phi$  is the phase. We note that a rotor representation of bosons  $b(\mathbf{x}) \sim \sqrt{\rho(\mathbf{x})} \exp[i\phi(\mathbf{x})]$  is possible when the healing length characterizing the characteristic length scale of density fluctuations is short compared to other length scales in the problem. Under the same conditions the density fluctuations are negligible if we are interested in long distance physics. In the superfluid phase this function shows algebraic scaling  $G(\mathbf{x}) \sim |\mathbf{x}|^{-\tau/4}$ , where the scaling exponent  $\tau$  is proportional to the temperature  $\tau \approx T/T_c$ , with  $T_c$  being the Kosterlitz-Thouless temperature. At the transition point we have  $G(\mathbf{x}) \sim |\mathbf{x}|^{-1/4}$ . Above the transition, the correlation function shows exponential scaling  $G(\mathbf{x}) \sim \exp(-|\mathbf{x}|/\xi)$ , with some correlation length  $\xi$ , which diverges near the transition temperature. The algebraic scaling of the superfluid phase is due to the thermally excited phonon (Bogoliubov’s) modes. In two dimensions these fluctuations generate quasilong-range order, rather than true long-range order. The transition to the exponential regime is due to vortex excitations. Above the transition, vortex-antivortex pairs are deconfined so that vortices and antivortices become unbound. These excitations generate a much more disordered phase field, which leads to exponential scaling of the correlation function.

If we couple the two superfluids with a hopping term in the temperature regime of the critical temperature, the system forms a phase-locked state, see Refs. [21,22]. Here the correlation function of the relative phase scales as

$G(\mathbf{x}) \sim \exp(-|\mathbf{x}|/\xi_i) + C$ , where  $C \neq 0$  and  $\xi_i$  is the correlation length of the phase-locked state. In this state the relative phase is well aligned over long distances; its fluctuations are strongly suppressed. We then turn off the hopping and study the evolution of the system.

In this article we show that the relaxational dynamics occur in two stages. The first fast stage, which we will term light cone relaxation, establishes a metastable quasi-equilibrium state of phonons (or Bogoliubov excitations) characterized by effective nonequilibrium temperature (in principle this metastable state can be completely nonthermal). During this stage the correlations between two arbitrary points in space  $\mathbf{x}_1$  and  $\mathbf{x}_2$ ,  $G(\mathbf{x}_1, \mathbf{x}_2, t)$ , where  $t$  is the time after the quench, initially decay in time, independent of their spatial separation  $x = |\mathbf{x}_1 - \mathbf{x}_2|$  because these points are not causally connected:  $G(\mathbf{x}_1, \mathbf{x}_2, t) \sim 1/t^\alpha$ , where  $\alpha$  is a power-law exponent related to the parameters of the system. At a later time  $t^*$ , when the condition  $2vt^* = x$  is fulfilled, these correlations (approximately) freeze in time so that  $G(\mathbf{x}_1, \mathbf{x}_2, t) \sim 1/x^\alpha$ . The exponent  $\alpha$  thus defines the nonequilibrium phonon temperature in the system. Because this first stage of dynamics involves only phonons, the exponent  $\alpha$  can exceed the maximally allowed equilibrium value of one-fourth, leading to a nonequilibrium supercritical metastable state, which can be thought of as a supercritical superfluid. It is analogous to an overheated classical liquid, for which a liquid state can be sustained above the critical temperature if the creation of defects is avoided. We find that the power law can be substantially above the critical scaling, and furthermore, that this metastable can be very long lived.

At longer time scales, vortex-antivortex pairs emerge and proliferate leading to the true equilibrium state. This process occurs at much longer time scales. We describe this thermalization process both numerically, using truncated Wigner approximation (TWA) and analytically. In particular, we show that thermalization (here corresponding to the process of vortex-antivortex proliferation) can be understood by extending renormalization group ideas to real time dynamics. By doing partial averaging over fast oscillating high-energy degrees of freedom, we can rewrite the equations of motion of slower degrees of freedom through renormalized coupling constants. As in the case of equilibrium systems we observe two possible scenarios corresponding to vortex-antivortex pairs being irrelevant (superfluid phase) or relevant (normal phase). Thus we are able to see how the system relaxes to one of the phases in real time. Divergent time (and length) scales in equilibrium systems translate into divergent relaxation times required to reach thermalization in the nonequilibrium case.

Physically this decay of the metastable superfluid state to the new equilibrium is very reminiscent of the Kibble-Zurek (KZ) effect [23,24]. The latter describes a ramp across a phase transition, starting on the disordered side. If the ordered state supports topological excitations, like vortices, then one expects very slow relaxation of the resulting state to the equilibrium due to vortex-antivortex recombination. This scenario is illustrated in Fig. 1(a): In the disordered phase we have excitations such as phonons, as well as topological defects. When we apply a fast ramp across the phase transition, the phonon excitations thermalize on very short time scales, while topological defects can exist on much longer time scales. The mechanism of

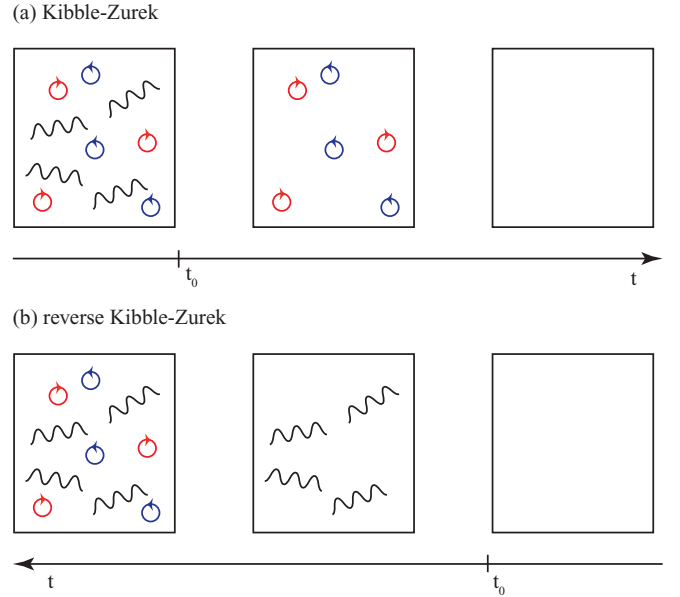


FIG. 1. (Color online) Illustration of the Kibble-Zurek (KZ) mechanism, which describes ramping across a phase transition from the disordered phase and its counterpart, the reverse-Kibble-Zurek (rKZ) effect. The latter describes ramping across a transition from the ordered side. Its defining feature is the dynamical suppression of vortex unbinding, which happens on a much longer time scale than the appearance of phononic excitations. We propose to study the rKZ in a bilayer of 2D superfluids of ultracold atoms by decoupling the superfluids and measuring the dynamics of the relative phase.

relaxation in our case is exactly complimentary and can be termed as a reverse Kibble-Zurek effect. Here, the ramp across a phase transition starts from the ordered side, as illustrated in Fig. 1(b). In the ordered phase both phonon excitations and vortices are suppressed. When the system is ramped across the transition, phonons are generated on a fast time scale. However, vortices are generated at much longer time scales leading to the long-lived supercritical superfluid state. We point out that, in thermally isolated systems (like cold atom systems), it is much easier to observe the reverse KZ effect because the disordered phase usually corresponds to a higher temperature. In isolated systems it is relatively easy to increase temperature by quenching some parameter, while decreasing temperature requires much more effort and can be done only in open systems.

This article is organized as follows: In Sec. II we introduce the numerical method that we use and find that at short time scales the system shows light cone dynamics. In Sec. III we consider the linearized dynamics of the bilayer system. Within this approximation both light cone dynamics and the emerging superfluid state can be understood. In Sec. IV we study the light cone dynamics of a solvable model, the transverse Ising model. In Sec. V we study dynamical vortex unbinding both with truncated Wigner approximation and with a renormalization group approach. We note that a short version of this article with some of the results was published earlier [25]. Here we expand the earlier treatment, present additional results and derivations, and formulate the real-time renormalization group approach that explains the numerical results.

## II. MICROSCOPIC MODEL AND THE TRUNCATED WIGNER APPROXIMATION

In this section we present the model that we use in our numerical approach. We consider two 2D (quasi)condensates that are aligned in parallel to each other that are coupled by a hopping term which is then turned off. This can be achieved by increasing the potential between the two condensates. The coarse-grained Hamiltonian describing the relative phase  $\phi_i$  of the two superfluids corresponds to an  $XY$  model, to which we add a hopping term to describe the phase-locking in the initial state

$$H = \Omega_0 \left[ - \sum_{\langle ij \rangle} \frac{\kappa}{\pi} \cos(\phi_i - \phi_j) + \frac{\pi}{2\kappa} \sum_i n_i^2 - V(t) \sum_i \cos(\sqrt{2}\phi_i) \right], \quad (1)$$

where  $\Omega_0$  is an overall (Josephson) energy scale and  $\kappa$  describes the ratio of kinetic and potential energies. We can formally replace these parameters by  $\Omega_0\kappa/\pi = 2Jn$ ,  $\pi\Omega_0/\kappa = U$  (so that  $\Omega_0 = \sqrt{2JnU}$ ,  $\kappa = \pi\sqrt{2Jn/U}$ ) and  $V(t) = 2J_\perp(t)n/\Omega_0$ , which gives a representation of two coupled Bose-Hubbard systems in the quantum rotor limit [26]. In this limit the Bose operators are replaced by the phase-density representation and the fluctuations of density are assumed to be small. In the Bose-Hubbard model  $J$  is the in-plane hopping amplitude,  $U$  is the on-site interaction energy,  $n$  is the filling number (i.e., the number of particles per site) and  $J_\perp$  is the interlayer hopping amplitude  $J_\perp$ . This representation gives, at best, a qualitative idea of how the model parameters relate to the parameters in the experiment, but gives a more intuitive picture. We note that one can think about the continuum limit as discrete, where the lattice constant is approximately given by the zero-temperature healing length in the system (i.e., the length over which density fluctuations are suppressed).

We emphasize that despite the Berezinskii-Kosterlitz-Thouless (BKT) transition being classical in origin (i.e., driven by thermal fluctuations) the mechanism of vortex or phonon creation in the process we consider comes from quantum fluctuations. Indeed when the superfluids are strongly coupled together the density (which plays the role of momentum conjugate of the phase) strongly fluctuates because of the zero point motion. The heating mechanism of this system can be thought of as an enhancement of this zero point motion following the quench.

It is convenient to introduce the rescaled quantities  $\tilde{t} = \Omega_0 t/\hbar$ ,  $\tilde{\phi} = \sqrt{\frac{\kappa}{\pi}}\phi$  and  $\tilde{n} = \sqrt{\frac{\pi}{\kappa}}n$ . In terms of these, the classical equations of motion (EOM's) are

$$\frac{d\tilde{\phi}_i}{d\tilde{t}} = -\tilde{n}_i \quad (2)$$

$$\frac{d\tilde{n}_i}{d\tilde{t}} = -\frac{\sqrt{2}}{\beta} \sum_{j_i} \sin\left(\frac{\beta(\tilde{\phi}_{j_i} - \tilde{\phi}_i)}{\sqrt{2}}\right) + V(t)\beta \sin \beta \tilde{\phi}_i, \quad (3)$$

where we defined  $\beta = \sqrt{2\pi/\kappa}$ . The indices  $j_i$  describe the four neighboring sites of site  $i$ .

We model the relative phase using a numerical implementation of the truncated Wigner approximation (TWA) (see Ref. [27] for a review): The expectation of any quantity at

some time  $t > 0$  can be determined by sampling over a Wigner distribution at time  $t = 0$  and solving the classical equations of motion from 0 to  $t$ . This approximation is guaranteed to be accurate at short times [28,29]. This approximation is also exact for any quadratic theory so we expect it to be accurate in the first (light cone) stage of dynamics primarily driven by phonon excitations. In our case we expect that TWA is also valid at longer times because when vortex-antivortex pairs start to emerge the system already reached the metastable state corresponding to the finite effective temperature. At this point quantum fluctuations become suppressed by much stronger thermal fluctuations driving the slow vortex dynamics.

We solve these EOM's for initial conditions that are distributed according to the Wigner distribution at  $t = 0$ . We can calculate this distribution under the assumption that  $J_\perp$  is larger than the other energy scales at  $t = 0$ . In this limit the phase fluctuations are small and can be described within the Bogoliubov approximation, where the system reduces to a sum of oscillators. The Fourier modes  $\tilde{\phi}_q$  and  $\tilde{n}_q$  at  $t = 0$  are distributed according to (see Ref. [29])

$$W \sim \exp\left(-\frac{\tilde{\phi}_q^2}{2\sigma_q^2 r_q} - \frac{2\sigma_q^2 \tilde{n}_q^2}{r_q}\right), \quad (4)$$

where  $\sigma = 1/\sqrt{2\omega_q}$ ,  $r_q = \coth(\omega_q/2T_0)$ , and  $\omega_q = \sqrt{4\sin(q_x/2)^2 + 4\sin(q_y/2)^2 + V\beta^2}$ , with  $T_0$  being the initial temperature. Note that, formally,  $\omega_q$  diverges at  $V \rightarrow \infty$ . This divergence is unphysical, being an artifact of using Hamiltonian (1) in the number phase representation. In reality when  $J_\perp$  becomes very large the transverse Josephson frequency saturates at  $\omega \approx 2J_\perp$ . This happens at  $V \sim n$  or equivalently  $J_\perp \sim Un$ . So for very strong initial coupling one can still use distribution (4) with  $V \rightarrow n$ .

To visualize our simulations we show an example for a single run of the system on a 20-by-20 lattice in Fig. 2. The direction of the arrows on each lattice point describe the phase  $\phi_i$ . We show “snapshots” at various times. The plaquettes around which there is a phase winding of  $\pm 2\pi$  are marked as vortices and antivortices. We see that, at  $t = 0$ , the phases are well aligned due to the coupling between the layers, with some small quantum fluctuations described by the Wigner function. The coupling is then turned off, vortices and antivortices are created pairwise, and unbind on a long time scale, as we will discuss further on. To extract expectation values of our observables from our simulations, we have to average them over many realizations of initial fluctuations.

We use this method to extract the equal time correlation function

$$G(x, t) = \langle \exp[i\sqrt{2}\phi_j(t) - i\sqrt{2}\phi_{j+x}(t)] \rangle, \quad (5)$$

where  $x$  is an integer separation between the points and  $t$  is the time after decoupling (see Fig. 3). Because we are using periodic boundary conditions  $G(x, t)$  depends only on the separation between the points  $x$  and does not depend on  $j$ . Note that this correlation function [or rather  $\int_0^x dx' G(x', t)$ ] can be directly measured in interference experiments [5,17,30]. We indeed see a very clear emergence of the light cone thermalization: At separations larger than  $2vt$ , where  $v$  is the characteristic phonon velocity,  $G(x, t)$  is almost  $x$  independent—it uniformly decreases in time. Once  $2vt > x$

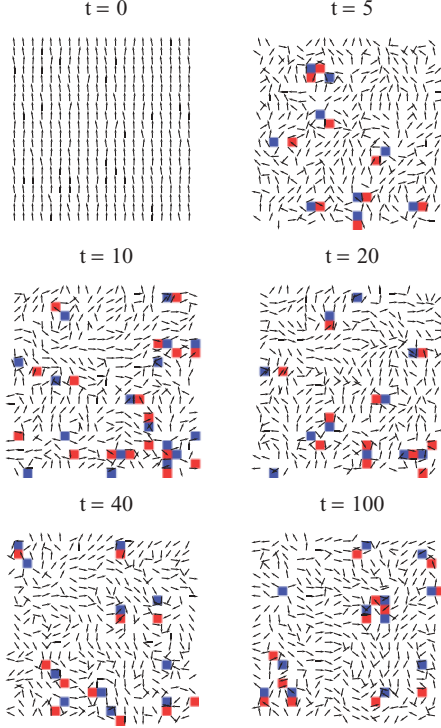


FIG. 2. (Color online) We simulate the dynamics of the relative phase of two 2D superfluids by solving the equations of motion and by averaging over the Wigner distribution of the initial state. A single run is shown here for  $V = 100$ ,  $\kappa = 10$ , and  $T = 2$ , at the times  $t = 0, 5, 10, 20, 40, 100$ . Vortices are marked red, antivortices blue.

the correlations freeze in time and depend only on  $x$ . The quantities in the system were rescaled such that the phonon velocity is set to 1.

We find that the state that emerges within the light cone shows algebraic scaling and therefore can be referred to as a superfluid.

### III. LINEARIZED DYNAMICS

In this section we study the linearized dynamics of the system. Within this description, both the light cone dynamics and the metastable superfluid (SF) state can be understood. The quadratic Hamiltonian describing the relative phase of

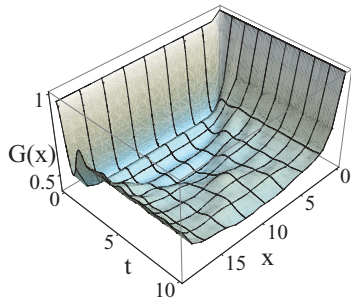


FIG. 3. (Color online) Plot of short-time behavior of the correlation function as a function of time and space, at temperature  $T = 3$ , for  $\kappa = 10$  and  $V = 20$ . The dynamics separate into instantaneous, damped oscillatory behavior, and a “light cone”-like pulse.

two coupled superfluids reads

$$H_0 = \int d^2r \left( -\frac{v}{2r_0} (\nabla\phi)^2 + \frac{g_{\perp}}{2} \phi^2 + \frac{vr_0}{2} n^2 \right). \quad (6)$$

$v$  is the phonon velocity of the SF, approximately given by  $v = \sqrt{gn/m}$ .  $r_0$  is the short-range cutoff of the system, of the order of the healing length.  $J = v/r_0$  is the KT energy. The term  $g_{\perp}\phi^2/2$  is created by the hopping term of the bilayer. It is approximately given by  $g_{\perp} = 4J_{\perp}n$ . We note that when this Hamiltonian is put on a lattice with a lattice constant  $r_l$  we obtain

$$H_1 = \Omega_0 \sum_i \left( -\frac{r_l}{r_0} \sum_{j_i} \frac{(\phi_i - \phi_{j_i})^2}{2} + \frac{g_{\perp}r_l^2}{2\Omega_0} \phi_i^2 + \frac{r_0}{2r_l} n_i^2 \right). \quad (7)$$

This expression can be also obtained directly linearizing the original Hamiltonian (1). The index  $j_i$  here describes the four neighboring sites of the site  $i$  and  $n_i$  is the filling fraction, related to the density via  $n_i = nr_l^2$ .  $\Omega_0$  is related to the phonon velocity as  $\Omega_0 = v/r_l$ . We therefore find that the squeezing parameter  $\kappa/\pi$  is given by  $\kappa/\pi = r_l/r_0$ , that is, it is the ratio of the discretization length scale  $r_l$  and the short-range cutoff  $r_0$  of the system.  $g_{\perp}$  is related to  $V(t)$  by  $g_{\perp}r_l^2/2 = \Omega_0 V(t)$ .

We now consider the time evolution of  $\phi$  and  $n$  under Eq. (6). It is convenient to go to a momentum representation where different modes decouple from each other. Assuming also that we are interested in momenta smaller than  $1/r_l$ , where the lattice effects are not important, we obtain the following equations of motion

$$\frac{d}{dt} n_k = -\Omega_0 \left( \frac{r_l \epsilon_k^2}{r_0} + 2V \right) \phi_{-k}, \quad (8)$$

$$\frac{d}{dt} \phi_k = \Omega_0 \frac{r_0}{r_l} n_{-k}, \quad (9)$$

where  $\epsilon_k^2 = 4 \sin^2 k_x/2 + 4 \sin^2 k_y/2$  and  $k$  is dimensionless,  $k = -\pi \dots \pi$ .

We rescale the time variable as  $\tilde{t} = \Omega_0 t/\hbar$ . The initial dispersion is then given by

$$\omega_{k,0}^2 = \epsilon_k^2 + 2Vr_0/r_l. \quad (10)$$

The dispersion  $\omega_k$  after the quench is simply  $\omega_k^2 = \epsilon_k^2$  in these units. We solve these equations and calculate the equal-time correlation function at time  $t$  after the quench. We use

$$G(\mathbf{x}, t) = \langle \exp[i\phi(\mathbf{0}, t)] \exp[-i\phi(\mathbf{x}, t)] \rangle \quad (11)$$

$$= \exp(-\langle \delta\phi^2 \rangle/2), \quad (12)$$

where  $\delta\phi = \phi(\mathbf{0}, t) - \phi(\mathbf{x}, t)$ . The averaging is now trivially done using the Wigner distribution (4). If we put the system back to the lattice we then find

$$\begin{aligned} \langle \delta\phi^2 \rangle &= \sum_{\mathbf{k}} (2 - 2 \cos \mathbf{k} \cdot \mathbf{x}) \\ &\times \left( \frac{r_{k,0}}{2\omega_{k,0}} \cos^2(\omega_k t) + \frac{r_{k,0}\omega_{k,0}}{2\omega_k^2} \sin^2(\omega_k t) \right). \end{aligned} \quad (13)$$

The quantities  $r_{k,0}$  and  $\omega_{k,0}$  are defined as before.

We now calculate the Green's function in the linearized regime numerically using Eqs. (12) and (13). We choose the



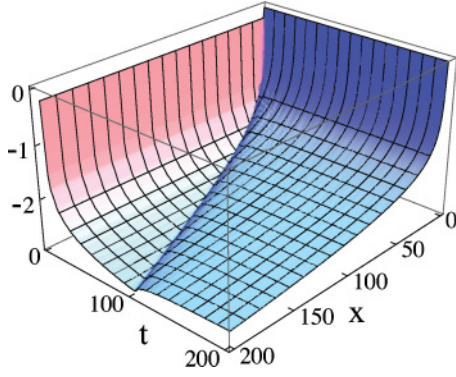


FIG. 4. (Color online)  $\langle \delta\phi^2 \rangle$  of the linearized system, for  $T = 1$  and  $V\beta^2 = 20$ , as a function of the lattice site, and  $vt$ .

discretization  $r_l = r_0$ , the initial temperature  $T/\Omega_0 = 1$ , and the initial coupling  $V\beta^2 = 20$ . In Fig. 4 we plot  $\langle \delta\phi^2 \rangle$  and in Fig. 5 we plot the correlation function. In both plots the light cone dynamics are clearly visible. Because of the translational invariance the correlation function that emerges in the light cone only depends on the relative distance is given by

$$G(\mathbf{x}, t) \approx C_1 |x|^{-T^*/4T_{KT}}, \quad (14)$$

for  $x \ll 2vt$ , where  $T^*$  is an effective temperature that is estimated below and  $C_1$  is a numerical prefactor. Outside of the light cone ( $x \gg 2vt$ ) the function  $G(\mathbf{x}, t)$  only depends on time  $t$  but not on the distance  $\mathbf{x}$

$$G(\mathbf{x}, t) = C_2 |t|^{-T^*/4T_{KT}}, \quad (15)$$

where  $T^*$  is the same effective temperature. At the light cone boundary  $x \approx 2vt$  the two asymptotics for the correlation functions (14) and (15) approximately coincide. However, we note that the prefactor  $C_2$  is in general different from  $C_1 v^{-T^*/4T_{KT}}$  as it is evident from the existence of a wave front that is visible in Figs. 4 and 5.

The temperature that emerges inside the light cone can be estimated by considering the quadratures of  $\phi$  at long times

$$\langle \phi_k^2(t \rightarrow \infty) \rangle = \frac{r_{k,0}}{4\omega_{k,0}} + \frac{r_{k,0}\omega_{k,0}}{4\omega_k^2}. \quad (16)$$

We find that the whole Wigner function in the noninteracting evolution remains Gaussian. It means that for each mode the

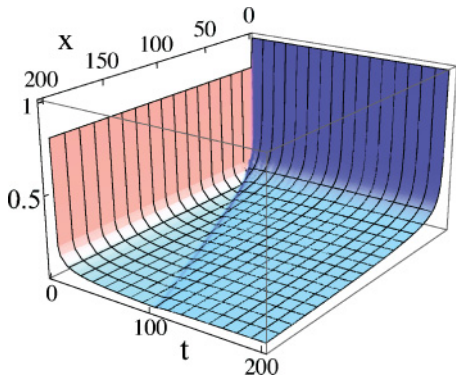


FIG. 5. (Color online) The correlation function of the linearized system, for  $T = 1$  and  $V\beta^2 = 20$ , as a function of the lattice site, and  $vt$ .

Wigner function is equivalent to that of a harmonic oscillator at finite “temperature”  $T_k^*$ , which is in general mode-dependent

$$\frac{r_k^*}{\omega_k} = \frac{r_{k,0}}{2\omega_{k,0}} + \frac{r_{k,0}\omega_{k,0}}{2\omega_k^2}, \quad (17)$$

where  $r_k^* = 1/\tanh(\omega_k/2T_k^*)$ . Solving for  $T_k^*$  gives

$$T_k^* = \frac{\omega_k}{2 \tanh^{-1} \left( \frac{2\omega_k\omega_{k,0}}{\omega_k^2 + \omega_{k,0}^2} \tanh(\omega_{k,0}/2T) \right)}. \quad (18)$$

For large  $V\beta^2$ , which corresponds to initially strong coupling between two superfluids, this simplifies to a single value, independent of  $k$

$$T^* = \frac{\sqrt{V\beta^2}}{4 \tanh(\sqrt{V\beta^2}/2T)}. \quad (19)$$

For small initial temperatures  $T$  we have  $T^* \approx \sqrt{V\beta^2}/4$  ( $T^* = 2J_\perp/J$  in terms of the original Hubbard parameters), that is, the temperature is fully determined by the initial coupling energy. The coupling energy between the two layers is transferred into the in-plane kinetic energy. We remind again that this result is valid as long as  $J_\perp \lesssim Un$ , otherwise the dependence of  $T^*$  on  $J_\perp$  saturates and for the infinite coupling limit we have  $T^* \sim Un/J$ . For large  $T$  we have  $T^* \approx T/2$ . This result is a reflection of the doubling of the degrees of freedom when two layers are uncoupled. In Fig. 6(a) we show dependence  $T^*(T)$  evaluated according to Eq. (19), for  $V = 20$ , and for  $\kappa = 1, 3, 10$  corresponding to lowering  $J_\perp$ . For  $\kappa = 1$ ,  $T^*$  is always above the critical temperature  $T_c = \pi/2$ , for  $\kappa = 10$ , it crosses it. We therefore expect to see very little vortex formation for small temperatures for  $\kappa = 10$  and many vortices for all temperatures for  $\kappa = 1$ . The intermediate value  $\kappa = 3$  approximately describes the transition between these limits.

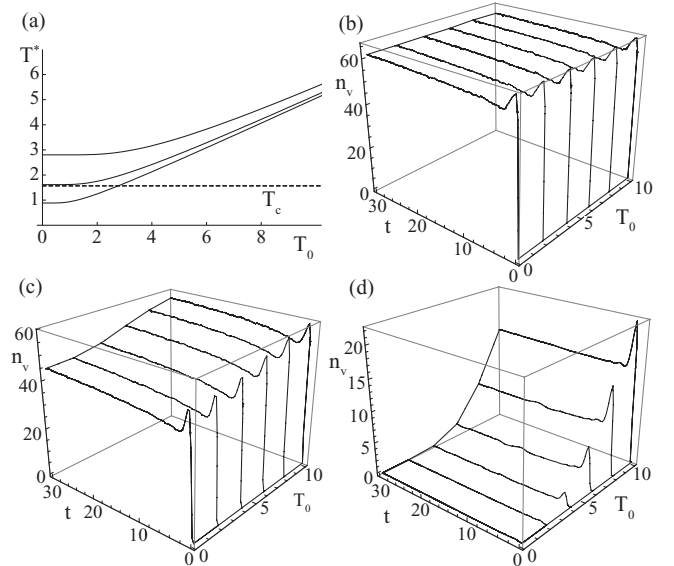


FIG. 6. (a)  $T^*$ , as given in Eq. (19), for  $\kappa = 1, 3, 10$ , from top to bottom and for  $V = 20$ . The line  $T_c = \pi/2$  was added to indicate the critical temperature. (b)–(d) Simulations for these values of  $\kappa$  and  $V$ . We plot the number of vortices  $n_v$  as a function of time  $t$  and initial temperature  $T_0$ .

To make this point more clearly, in Fig. 6(b)–6(d) we plot full nonlinear TWA simulation for each of the three cases. We run the quench for different temperatures  $T$ , and plot the number of vortices  $n_v$  in the system as a function of time. This number is obtained by counting the vortices (indicated by red plaquettes in Fig. 2), and then by averaging over many runs. We find that for  $\kappa = 1$ , the number of vortices is virtually unchanged implying that the dynamics are completely dominated by quantum fluctuations, whereas for  $\kappa = 10$  this number drops to zero when the temperature is lowered. These results are consistent with the emergent temperature  $T^*$  obtained within the linearized approach.

#### IV. LIGHT CONE DYNAMICS IN THE TRANSVERSE ISING MODEL

In this section we demonstrate that light cone dynamics are not just characteristic for the system we are interested in, which is characterized by low-energy bosonic wave excitations. The same mechanism of reaching a steady state is much more general and is likely related to the existence of the maximum group velocity in Schrödinger systems as was proven by Lieb and Robinson [31]. In this section we demonstrate the presence of the light cone dynamics in another solvable model, the transverse Ising chain [26,32] described by the Hamiltonian

$$H_I = -J_I \sum_i (\sigma_i^x \sigma_{i+1}^x + g \sigma_i^z), \quad (20)$$

where  $J_I$  is an overall energy scale,  $g$  describes the strength of the transverse field, and  $\sigma^{x,z}$  are the Pauli matrices. We follow the calculational procedure in Ref. [26]. First, we use a Jordan-Wigner transformation

$$\sigma_i^z = 1 - 2n_i, \quad (21)$$

$$\begin{aligned} \langle n_i(t) n_j(t) \rangle = \frac{1}{M^2} \sum_{k_1, k_2} \{ & \exp[-i(k_1 - k_2)(r_i - r_j)] [v_{k_1, g}^2 + F_{g, g'}(k_1, t)] [u_{k_2, g}^2 - F_{g, g'}(k_2, t)] \\ & + [u_{k_1, g} v_{k_1, g} + G_{g, g'}(k_1, t)] \\ & \times [u_{k_2, g} v_{k_2, g} + G_{g, g'}^*(k_2, t)] + [v_{k_1, g}^2 + F_{g, g'}(k_1, t)] [v_{k_2, g}^2 + F_{g, g'}(k_2, t)] \}, \end{aligned} \quad (28)$$

where

$$G_{g, g'}(k, t) = \left( i \sin(2\epsilon_{k, g} t / \hbar) + \frac{1}{2} \frac{[\cos(2\epsilon_{k, g} t / \hbar) - 1](g' - \cos k)}{\sqrt{g'^2 - 2g' \cos k + 1}} \right) \left( \frac{(g' - g) \sin k}{\sqrt{(g^2 - 2g \cos k + 1)(g'^2 - 2g' \cos k + 1)}} \right). \quad (29)$$

Using these expressions we can easily analyze the quench dynamics. In Fig. 7 we show two examples showing spin-spin (density-density) correlation functions after a quench. The first example corresponds to the ramp from  $g = 3$  to  $g' = 1$  (i.e., a quench to the quantum critical point). At this point the dispersion (24) becomes gapless and linear at small energies. Then the light cone dynamics are anticipated because there is a well defined “speed of light” characterizing the propagation of excitations, which is equal to  $2J$ . Indeed Fig. 7(a) shows a clear signature of such dynamics. There is a clearly visible “light cone,” which separates into an instantaneous part (connecting not causally connected points)

$$\sigma_i^x = \prod_{j < i} (1 - 2n_j) (c_i + c_i^\dagger), \quad (22)$$

where  $c_i$  are Fermi operators and  $n_i = c_i^\dagger c_i$ . This transformation leads to a fermionic representation of the Hamiltonian that can be further diagonalized using the Bogoliubov transformation

$$\gamma_{k, g} = u_{k, g} c_k - i v_{k, g} c_{-k}^\dagger, \quad (23)$$

where  $c_k$  is the Fourier transform of  $c_i$ ,  $u_{k, g}$  and  $v_{k, g}$  are given by  $\cos(\theta_{k, g}/2)$  and  $\sin(\theta_{k, g}/2)$ , where  $\theta_{k, g} = \arctan(\sin k / (g - \cos k))$ . The resulting dispersion is

$$\epsilon_{k, g} = 2J_I \sqrt{g^2 - 2g \cos k + 1}. \quad (24)$$

We consider a time dependent  $g(t)$ . For  $t < 0$  we have  $g(t) = g$  and we assume the system to be in equilibrium. We then assume that for  $t > 0$ ,  $g(t)$  jumps to the value  $g'$ . The equal-time correlation function of  $\sigma_i^z$  can be calculated exactly by expressing it in terms of the operator  $n_i$  [i.e.,  $\langle \sigma_i^z(t) \sigma_j^z(t) \rangle = 1 - 4\langle n_i(t) \rangle + 4\langle n_i(t) n_j(t) \rangle$ ]. It can be shown that the average density fermionic density (corresponding to the  $z$  component of the magnetization) is given by

$$\langle n_i(t) \rangle = \langle n_i(0) \rangle + \frac{1}{M} \sum_k F_{g, g'}(k, t), \quad (25)$$

with

$$F_{g, g'}(k, t) = \frac{[\cos(2\epsilon_{k, g} t / \hbar) - 1/2](g' - g) \sin^2 k}{\sqrt{g^2 - 2g \cos k + 1}(g'^2 - 2g' \cos k + 1)}, \quad (26)$$

and

$$\langle n_i(0) \rangle = \frac{1}{2} - \frac{1}{2M} \sum_k \frac{g - \cos k}{\sqrt{g^2 - 2g \cos k + 1}}. \quad (27)$$

In turn the density-density correlation function  $\langle n_i(t) n_j(t) \rangle$  reads

that is independent of the distance, and a spatially dependent (causal) part, that expands in the form of a wave front. In Fig. 7(b) we use  $g' = 0.5$ , where at low energies the spectrum of excitations is gapped. Although the dispersion in this model is linear (relativistic) only at sufficiently high energies above the gap we still see a clear light cone structure. The expansion velocity of the “light cone” in this case is consistent with twice the maximum of the group velocity  $v_{gr}(k) = d\epsilon/dk$  given by

$$v_{gr, \max} = \begin{cases} 2Jg & \text{for } |g| < 1 \\ 2J & \text{for } |g| \geq 1. \end{cases} \quad (30)$$

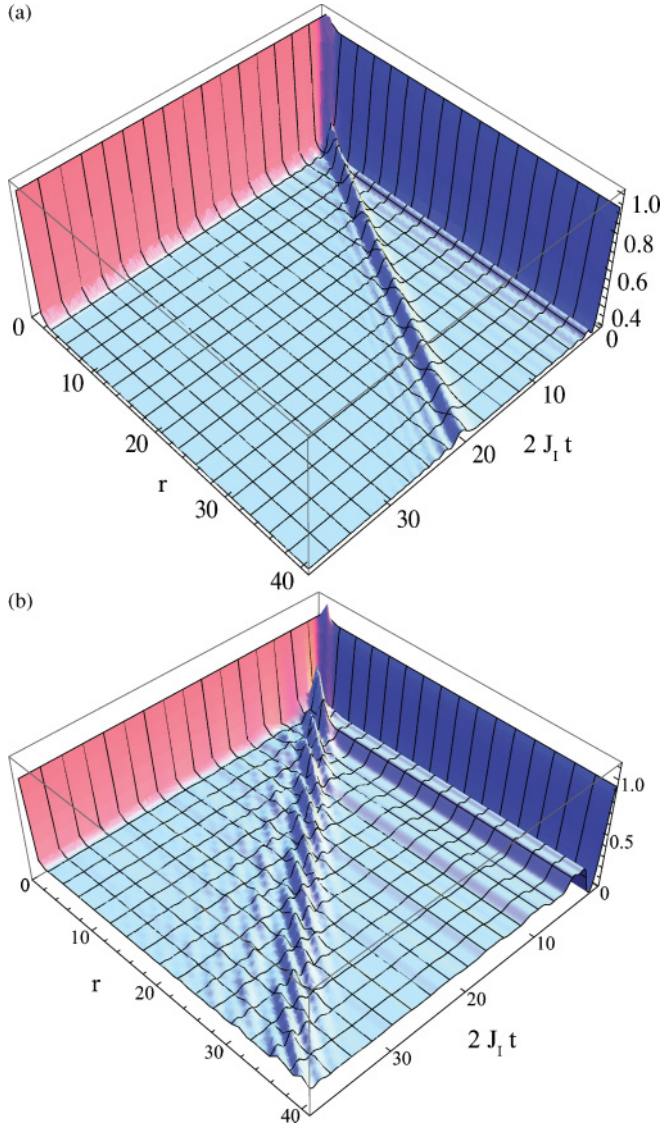


FIG. 7. (Color online) The correlation function  $\langle \sigma_0^z(t) \sigma_r^z(t) \rangle$  for a quench from  $g = 3$  to  $g' = 1$ , in (a) and from  $g = 3$  to  $g' = 0.5$  in (b), as a function of time  $t$ , specifically of  $2J_1 t$ , and the spatial distance  $r$ .

So for  $g' = 1$  we find  $2v_{gr,max} = 4J$  and for  $g' = 0.5$  we find  $2v_{gr,max} = 2J$ . These are indeed the expansion velocities that we see in Fig. 7.

## V. DYNAMICAL VORTEX UNBINDING

In this section we address the important question of how the supercritical state relaxes to the ground state (i.e., the second stage of the dynamics). As we mentioned in the Introduction the anticipated mechanism for this relaxation is vortex unbinding. This process is intrinsically nonlinear and requires a more sophisticated treatment than that of the noninteracting “light cone” dynamics. In this work we use two complimentary approaches. In Sec. V A we use a numerical implementation of the TWA to simulate the dynamics in the system. In Sec. V B we generalize a renormalization group approach to analytically describe the process of relaxation in real time.

### A. Numerical approach

Within TWA we need to solve the full nonlinear equations of motion (3) subject to the initial conditions distributed according to the Wigner function (4). Then the equal-time correlation functions or other observables are found by averaging the Weyl symbol of the corresponding observable computed at time  $t$  over the fluctuating initial conditions. Note that since we are interested only in the phase-phase correlation function, the corresponding Weyl symbol is obtained by simply substituting the Heisenberg quantum operator corresponding to the phase with the classical phase [29]. In Fig. 8 we show the result of such simulations. We can observe how the metastable superfluid state relaxes to the disordered state. For that we show the correlation functions of the system on a much longer time scale than in Fig. 3. The exponent of the algebraic scaling gradually decreases. Eventually the correlation function is more accurately approximated by an exponential fitting function, signaling that the thermal Bose gas phase was reached. Because this is the phase of deconfined vortices and because the intermediate superfluid phase is well described by a phonon-only description, we conclude that the dynamical transition that we observe is due to vortex unbinding. The example of a single run shown in Fig. 2 is consistent with this picture: Defects are created soon after the quench, but they only gradually separate on a much longer times scale. It is this process that we refer to as the reverse Kibble-Zurek mechanism.

To better characterize the process of vortex unbinding further we fit the correlation function  $G(x, t)$  to either algebraic or exponential fitting functions. Such a choice is motivated by the two possible regimes of the equilibrium system and is supported by the analytic renormalization group results presented in the next section. The algebraic fitting function we use is  $c[L/\pi|\sin(\pi x/L)|]^{-\tau/4}$  and the exponential function is  $c \exp[-|\sin(\pi x/L)|/x_0]$ . Note that in the fitting functions we use the conformal distance  $L/\pi|\sin(\pi x/L)|$ , which is more appropriate in finite systems with periodic boundary conditions (see e.g. Ref. [26]). In equilibrium the algebraic exponent  $\tau$  will be the relative temperature  $T/T_c$ . Any value above 1 is therefore supercritical. The parameter  $x_0$  defines the length scale of the exponential decay. The parameter  $c$  in both functions gives an overall scale.

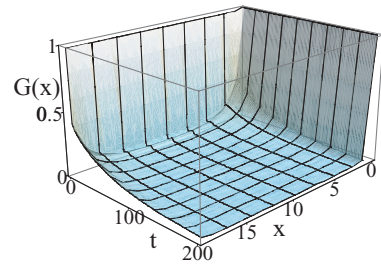


FIG. 8. (Color online) Long-time behavior of the correlation function for  $T = 1$ ,  $\kappa = 8$ , and  $V = 80$ . The correlation function first develops algebraic scaling, so the system forms a metastable quasisuperfluid state. On longer time scales the correlation function shows exponential decay. The coherence is lost due to dynamical vortex unbinding.



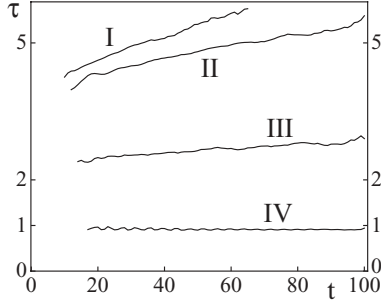


FIG. 9. Time dependence of the exponent  $\tau$  extracted from fitting the long-time correlation function  $G(x, t)$ , for different initial couplings. In all four examples we use  $T = 1$  and  $\kappa = 8$ . The initial couplings  $V$  are chosen as  $V = 80, 70, 50$ , and  $20$ , corresponding to curves I to IV. The curve I corresponds to the example shown in Fig. 8. In this case the correlation function can be well fitted with an algebraic function for up to  $t \approx 60$ , after that  $G(x, t)$  is better fitted by an exponential function with a decay length of the order of the lattice constant. For the other cases,  $G(x, t)$  is well fitted with an algebraic function throughout the whole time interval.

Using these fitting functions we analyze four different situations corresponding to the same initial temperature  $T = 1$  and the same parameter  $\kappa = 8$ , but with different initial couplings  $V$  between the planes. The first (I) case corresponding to  $V = 80$  is identical to the one plotted in Fig. 8. The other three curves correspond to  $V = 70, 50, 20$  (II–IV). In Fig. 9 we show the exponent  $\tau$  extracted from the fit as a function of time for these situations. In all of them at short times  $G(x, t)$  develops algebraic scaling when the light cone dynamics reaches the system boundaries. For the cases I–III the emerging scaling exponent  $\tau$  is well above the critical exponent. After that, the exponent gradually increases on much longer time scales. During this process, the decay of the correlation function is still fitted well with the algebraic function. Eventually the algebraic scalings breaks down and  $G(x, \tau)$  develops exponential scaling, indicating vortex unbinding. This regime of exponential scaling is reached for  $V = 80$  (I) within the time interval shown in Fig. 9. For  $V = 70$  (II) and  $V = 50$  (III) the time scale of the vortex unbinding is longer than the time interval shown. For  $V = 20$  (IV) the system equilibrates to the superfluid state. Because in this case the exponent  $\tau$  is less than 1, vortices never unbind and the algebraic scaling persists at all times. We conclude from these examples that there can be a sizable range of initial values of  $V$ , which generates the scenario of a supercritical superfluid, and of dynamically suppressed vortex unbinding. Furthermore, the algebraic scaling exponents that can occur in the metastable state are well above criticality and should be easily distinguishable from subcritical values. These supercritical exponents can be detected using interference experiments along the lines of Refs. [5,30].

## B. Renormalization group approach

In this section we develop the renormalization group (RG) approach to dynamical vortex unbinding. We find that the dynamical evolution of the system can be related to the RG flow of the *equilibrium* system. The idea of RG in real time

is quite similar in spirit to the RG in imaginary time. Namely our goal is to eliminate high-energy, high-momentum degrees of freedom. In equilibrium, this is done by the means of usual perturbation theory (or Gaussian integration), which is justified because of the large energy gap separating high-energy states from the low-energy degrees of freedom we are interested in. In real time the idea of renormalization is quite similar. High-energy (momentum) phonons are not very sensitive to slow processes leading to vortex formations. Thus these phonons can be well treated within the linearized approach. However, due to nonlinearities such phonons slightly renormalize the parameters governing dynamics of low-energy degrees of freedom. This renormalization is precisely what we are interested in. Note that technically in the RG procedure we perform averaging of the equations of motion over short times. Then odd powers of highly oscillating fields average to zero while averaging of the even powers gives some constant contribution. This contribution is precisely what renormalizes coupling constants governing the low temperature dynamics.

We point out that typical RG flow diagrams contain mostly nonequilibrium points, in fact, all except for the fixed points. As we saw in the previous sections, one can associate an effective temperature to the metastable state that emerges after the dephasing of the phonon modes. In turn with this effective parameter we can associate a location of the transient state in the RG flow of the equilibrium system. This effective temperature can then either gradually increase, until the system starts to show exponential scaling, or the system can always remain superfluid, if the algebraic scaling is subcritical and the effective temperature always remains below  $T_{KT}$ . This behavior resembles the equilibrium RG flow of a Kosterlitz-Thouless transition (which now occurs in real, not imaginary, time), on which we elaborate in this section.

Instead of directly analyzing the rotor model to describe the Kosterlitz-Thouless physics and vortex unbinding, we will work with the dual  $Z_1$  clock model (or equivalently 2D sine-Gordon model), described by the action

$$S = \int d^2r \left( \frac{\lambda}{2} (\partial_x \theta)^2 - \frac{g}{a^2} \cos \theta \right). \quad (31)$$

For the details of the duality transformation see Ref. [33]. The parameters of this model can be related to those of the XY model by

$$\lambda = \frac{1}{8\pi} \frac{T}{T_{KT}} = \frac{1}{4\pi^2} \frac{T}{J_{KT}} \quad (32)$$

$$\frac{g}{2} = \exp(-S_c), \quad (33)$$

where  $E_c = S_c T$  is the vortex core energy and  $\lambda$  is a measure of the relative temperature. We note that the action in Eq. (31) has a high-momentum cutoff  $\Lambda$ , which is the inverse of the short-range cutoff  $a$  (i.e., we set  $\Lambda a = 1$ ). To describe the dynamics of this model we use the effective 2D sine Gordon Hamiltonian

$$H/T = \int d^2r \left( \frac{\mu}{2} p^2 - \frac{\lambda}{2} (\partial_x \theta)^2 + \frac{g}{a^2} \cos \theta \right). \quad (34)$$



Here the parameter  $\mu$  is chosen, so that the dispersion of the linearized XY model is recovered

$$\mu = \frac{\omega_k^2}{\lambda k^2 T^2}, \quad (35)$$

which we also write as  $\omega_k = v|k|$ , where the velocity  $v$  is given by  $v = \sqrt{\mu\lambda T^2}$ . The nonlinear term  $\cos \theta$  in Eq. (34) describes the vortex field. If this term is important (large  $g$ ) then the field  $\theta$  localizes corresponding to a highly disordered phase of the dual field  $\phi$  (i.e., to the normal state). Conversely small  $g$  corresponds to the superfluid algebraic regime. The starting point of our RG analysis will be supercritical superfluid state, which emerges after the short-time light cone dynamics. Because the Kosterlitz-Thouless transition is classical in nature occurring at high temperatures the quantum fluctuations are no longer expected to be important and instead of the Wigner function as the new initial condition we can use its classical Boltzmann's limit. The initial state for the vortex dynamics, described by the effective temperature  $T$ , is thus fully characterized by the quadratures of the spectrum

$$\langle \theta_{\mathbf{k}}^* \theta_{\mathbf{k}} \rangle = \frac{1}{\lambda k^2}, \quad (36)$$

$$\langle p_{\mathbf{k}}^* p_{\mathbf{k}} \rangle = \frac{1}{\mu} = \lambda T^2 \frac{k^2}{\omega_k^2}. \quad (37)$$

The equations of motion corresponding to the Hamiltonian (34) are given by

$$\frac{d}{dt} p = \lambda T \partial_x^2 \theta + \frac{gT}{a^2} \sin \theta, \quad (38)$$

$$\frac{d}{dt} \theta = \mu T p. \quad (39)$$

We now apply the following renormalization procedure to these equations. We rescale the spatial and temporal variables as  $\mathbf{r} \rightarrow \mathbf{r}(1 + d\Lambda/\Lambda)$  and  $t \rightarrow t(1 + d\Lambda/\Lambda)$  and the  $p$  field as  $p \rightarrow p(1 - d\Lambda/\Lambda)$ . This implies that the momentum cutoff  $\Lambda$  is rescaled as  $\Lambda \rightarrow \Lambda' \equiv \Lambda(1 - d\Lambda/\Lambda)$ , so the momentum degrees of freedom between  $\Lambda'$  and  $\Lambda$  are removed. Without the nonlinear term in Eq. (38) these rescalings leave the equations of motion invariant. The linear dynamical evolution can therefore be considered to be the noninteracting fixed point of the RG. We now ask the question how this dynamical evolution is affected by the nonlinear term. Specifically we want to determine how the equations of motion behave at long times and distances. For this, we go beyond the bare rescaling and correct for the integrated-out degrees of freedom up to second order in  $g$ . The resulting flow equations are of the well-known BKT form

$$\frac{dg}{dl} = \left(2 - \frac{1}{4\pi\lambda}\right) g, \quad (40)$$

$$\frac{d\lambda}{dl} = \alpha \frac{g^2}{\lambda}, \quad (41)$$

where  $l = \ln \Lambda$  and  $\alpha$  is a nonuniversal prefactor. The RG step generated the equations of motion at time  $t'$  and distance  $r'$  from the equations at time  $t$  and distance  $r$ , with renormalized coefficients, according to Eqs. (40) and (41). Therefore the time dependence of the coefficients can be read off the solution of the RG flow, by realizing that:  $dt/dl = t$  or  $t = t_0 e^l$ . In

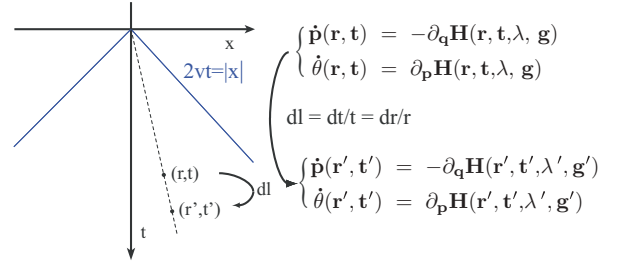


FIG. 10. (Color online) Schematic representation of a renormalization step in the real-time RG approach. In each step we renormalize simultaneously the space and time variables. This “moves” the equations of motion from  $(\mathbf{r}, t)$  to  $(\mathbf{r}', t')$ . We correct for the integrated-out degrees of freedom to second order in  $g$ , which renormalizes the parameters  $g$  and  $\lambda$  according to Eqs. (40) and (41).

Fig. 10 we show a schematic representation of our RG process. In the Appendix we discuss the derivation of the flow equations and give their more complete form.

One conclusion from Eqs. (40) and (41) is that the critical exponent of the dynamical process is equal to the one of the equilibrium system. We see from Eq. (40) that the critical value of  $\lambda$  is  $\lambda_c = 1/8\pi$ , which corresponds to  $T = T_{KT}$  as can be seen from Eq. (32). Another important observation is that the RG equations (40) and (41) predict a nonequilibrium analog of the BKT transition, where depending on the initial fluctuations in the system, the vortex-antivortex pairs can either unbind in the long time limit or remain bounded. This transition, as in the equilibrium case, is characterized by exponentially divergent time and length scales. Physically these divergencies correspond to a very slow process of equilibration of vortices near the nonequilibrium phase transition.

We can also use the RG flow to determine the time scale of vortex unbinding by using

$$g(t^*) \sim 1. \quad (42)$$

When  $T$  is well above  $T_{KT}$ , the time scale can be determined from Eq. (40)

$$t^* \sim \exp\left(\frac{E_c/2}{T - T_{KT}}\right), \quad (43)$$

where  $E_c = S_c T$ . Away from the transition, the time scale of vortex unbinding is therefore exponentially increased because of the energy cost given by the vortex core energy. Very close to the transition  $t^*$  scales as

$$t^* \sim \exp[\exp(-S_c/2)/\sqrt{1 - T_{KT}/T}]. \quad (44)$$

The time scale is renormalized because of the critical scaling in the vicinity of the transition.

## VI. CONCLUSION

In conclusion, we studied the dynamics of the relative phase of a bilayer of superfluids in 2D, after the hopping between them was turned off rapidly. We find that, on short time scales, the dynamics of the correlation function shows a “light cone”-like behavior. Depending on the parameters of the system, the light cone dynamics can result in a phase that shows supercritical algebraic scaling and can therefore be thought of as a superheated superfluid. On long time scales

the system relaxes to a disordered state via vortex unbinding, which constitutes a reverse-Kibble-Zurek mechanism. The properties of the dynamical process can be understood with a renormalization group approach. We find that the dynamical evolution of the system resembles the RG flow of the equilibrium system. In particular, using the RG equations we found two possible scenarios of the system reaching the steady state: (i) If initial quantum and thermal fluctuations are weak the vortices are irrelevant and long-time long-distance behavior is governed by the algebraic fixed point. The only role of vortices is then the renormalization of the superfluid stiffness and the sound velocity. (ii) If the initial fluctuations are strong then the vortices become relevant and proliferate resulting in a normal (nonsuperfluid) steady state. In this case RG gives the time scale of vortex unbinding, which exponentially diverges as the system approaches the nonequilibrium phase transition. The scaling that is given in Eqs. (43) and (44) can be interpreted as the extension of Kibble-Zurek scaling to sudden quenches (also see Ref. [34]). The behavior of the relative of the phase of two superfluids can be accurately studied by interference experiments of ultracold atom systems and therefore our predictions are of direct relevance to the experiment. In particular, the divergence of the thermalization time scale will suggest the feasibility of a nonequilibrium detection of the phase transition.

#### ACKNOWLEDGMENTS

We thank A. Castro Neto for useful discussions. The work of A.P. was supported by NSF DMR-0907039, AFOSR, and the Sloan Foundation. L.M. acknowledges support from NRC/NIST, NSF Physics Frontier Grant No. PHY-0822671 and Boston University's visitors program.

#### APPENDIX

In this Appendix we derive the RG Eqs. (40) and (41), which can also be written as a second-order differential equation for  $\theta$

$$\frac{1}{\mu} \frac{d^2}{dt^2} \theta = \lambda \Delta \theta + \frac{g}{a^2} \sin \theta. \quad (\text{A1})$$

To simplify the derivation, here and throughout the Appendix, we formally change notations  $\lambda T \rightarrow \lambda$ ,  $\mu T \rightarrow \mu$ , and  $g T \rightarrow g$ . The idea of momentum shell RG is that we treat high momentum components of  $\theta$  and  $p$  (or equivalently  $\dot{\theta}$ ) perturbatively, while not making any approximations about the low momentum components. Our goal is to find renormalization of the equations of motion governing the low momentum components. So we split

$$\theta(\mathbf{r}, t) = \theta^<(\mathbf{r}, t) + \theta^>(\mathbf{r}, t), \quad (\text{A2})$$

where the Fourier expansion of  $\theta^>(\mathbf{r}, t)$  only contains momenta in the shell  $\Lambda' \equiv \Lambda - \delta\Lambda < |k| < \Lambda$  and  $\theta^<(\mathbf{r}, t)$  contains all other Fourier components:

$$\theta^<(\mathbf{r}) = \frac{1}{\sqrt{V}} \sum_{k < \Lambda'} \exp(i\mathbf{k} \cdot \mathbf{r}) \theta_{\mathbf{k}}, \quad (\text{A3})$$

$$\theta^>(\mathbf{r}) = \frac{1}{\sqrt{V}} \sum_{\Lambda' < k < \Lambda} \exp(i\mathbf{k} \cdot \mathbf{r}) \theta_{\mathbf{k}}. \quad (\text{A4})$$

We will treat  $\theta^>$  (and correspondingly  $p^>$ ) perturbatively in  $g$  since the nonlinear term should only weakly couple to the high frequency field. We expand the high-momentum field as

$$\theta^>(\mathbf{k}, t) = \theta_0^>(\mathbf{k}, t) + \theta_1^>(\mathbf{k}, t). \quad (\text{A5})$$

Here  $\theta_0^>(\mathbf{k}, t)$  is the solution of the equations of motion, with  $g$  set to zero

$$\theta_0^>(\mathbf{k}, t) = \frac{\mu}{\omega_{\Lambda}} p_{0,\mathbf{k}}^> \sin(\omega_{\Lambda} t) + \theta_{0,\mathbf{k}}^> \cos(\omega_{\Lambda} t), \quad (\text{A6})$$

where  $\omega_k = v|k|$  and the velocity  $v$  is  $v = \sqrt{\lambda/\mu}$ . In the next leading order we have

$$\theta_1^>(\mathbf{k}, t) = \frac{g\omega_{\Lambda}}{\lambda} \int_0^t d\tau F_1(\mathbf{k}, \tau) \sin[\omega_{\Lambda}(t - \tau)], \quad (\text{A7})$$

where

$$F_1(\mathbf{k}, \tau) = \int d^2r \exp[-i\mathbf{k} \cdot \mathbf{r}] \sin[\theta_0^<(\mathbf{r}, \tau)], \quad (\text{A8})$$

and we used  $\Lambda a = 1$ . Note that in the last equation in the argument of the sinus we changed  $\theta_0$  to  $\theta_0^<$  because the contribution from  $\theta_0^>$  is smaller by the factor  $\delta\Lambda/\Lambda$ . So we see that in the leading order in  $g$  the high momentum component of  $\theta$  oscillates with time at very high frequency  $\omega_{\Lambda}$ . In the next order in  $g$  the high momentum component also acquires a low frequency component (as we will discuss below).

Next we consider the equation of motion (A1) expanding it up to the second order in  $\theta^>$

$$\begin{aligned} \frac{1}{\mu} \frac{d^2}{dt^2} \theta(\mathbf{r}, t) \approx & \lambda \Delta \theta(\mathbf{r}, t) + \frac{g}{a^2} \cos[\theta^<(\mathbf{r}, t)] \theta^>(\mathbf{r}, t) \\ & + \frac{g}{a^2} \sin \theta^<(\mathbf{r}, t) \left( 1 - \frac{[\theta^>(\mathbf{r}, t)]^2}{2} \right). \end{aligned} \quad (\text{A9})$$

Because of the nonlinearity high-momentum modes couple to the low-momentum modes leading to the renormalization of the couplings governing the dynamics of the latter. The idea of RG is to average equations of motion for low-momentum (slow) components over the fast oscillations. The averaging is trivially done in the last term of Eq. (A9). There it is sufficient to use zeroth order in  $\theta^>$ . Using that  $\overline{\sin^2(\omega_{\Lambda} t)} = \overline{\cos^2(\omega_{\Lambda} t)} = 1/2$  we find that averaging of the last term simply renormalizes the coupling  $g$

$$g \rightarrow g \left( 1 - \frac{\overline{E_{\Lambda}}}{4\pi\lambda} \frac{\delta\Lambda}{\Lambda} \right), \quad (\text{A10})$$

where  $\overline{E_k}$  is the average energy of the mode  $k$  over the period (we used the fact that  $\lambda k^2 |\theta_k|^2 = \overline{E_k}$ ). We note that in a Boltzmann ensemble, we will have  $\overline{E_k} = 1$  because the energies here are in units of the temperature  $T$ . With this assumption we will recover the flow equation of the equilibrium case.

Instead of this assumption, we proceed by noting that under RG transformations coupling constants slowly change in time. This implies that the adiabatic invariants per each mode are approximately conserved, as discussed in Ref. [35]. For an oscillator the adiabatic invariant is  $I_k = E_k/\omega_k$ . Thus we see that the energy of the mode is proportional to the frequency. Noting that at initial time  $\overline{E_k}(t=0) = 1$  (in nonrescaled

units this will be  $\overline{E_k}(t=0) = T_0$ , where  $T_0$  is the initial nonequilibrium temperature), one can rewrite Eq. (A10) as follows

$$g \left( 1 - \frac{1}{4\pi v_0} \frac{1}{K} \frac{\delta\Lambda}{\Lambda} \right), \quad (\text{A11})$$

where we introduced the analog of the Luttinger-Liquid parameter  $K = \sqrt{\lambda/\mu}$ .  $v$  is the velocity that is now given by  $v = \sqrt{\lambda\mu}$  (note that in the original, not rescaled units,  $v = T\sqrt{\lambda\mu}$ ).

Next let us consider the second term in Eq. (A9). This term is more subtle since if we use  $\theta_0^>$  the average over fast fluctuations will give zero. So we need to use the first correction  $\theta_1^>$ , which will be a correction at second order in  $g$ . We note that the linear term in Eq. (A9) can also be expanded to second in  $g$ , generating similar contributions. However, when written as Eq. (A1), such a term is canceled by a corresponding term from expanding  $d^2\theta/dt^2$ . Alternatively we can view Eq. (A9) as written for the  $\theta^<$  component, this automatically ensures that only the nonlinear term is responsible for the renormalization.

Let us look closer into the Eq. (A7). We are dealing with the integral over the fast oscillating function of  $\tau$ :  $\sin(\omega_\Lambda(t - \tau))$  and the slow oscillating function  $F$ . This integral can be evaluated by integrating by parts

$$\begin{aligned} & \int_0^t d\tau F_1(\tau) \sin[\omega_\Lambda(t - \tau)] \\ &= F_1(\tau) \frac{\cos[\omega_\Lambda(t - \tau)]}{\omega_\Lambda} \Big|_0^t \\ & - \frac{1}{\omega_\Lambda} \int_0^t d\tau \frac{dF_1(\tau)}{d\tau} \cos[\omega_\Lambda(t - \tau)]. \end{aligned} \quad (\text{A12})$$

Note that the second integral contains a large denominator  $1/\omega_\Lambda$ . In the first term only the limit  $\tau = t$  gives a nonoscillating contribution to the integral. We can continue the expansion in powers of  $1/\omega_\Lambda$ . Note that the next term proportional to  $\dot{F}_1$  will contain only highly oscillatory parts and can be neglected. So up to the third order in  $1/\omega_\Lambda$  we find

$$\int_0^t d\tau F_1(\tau) \sin[\omega_\Lambda(t - \tau)] \approx \frac{F_1(t)}{\omega_\Lambda} - \frac{1}{\omega_\Lambda^3} \frac{d^2 F_1(t)}{dt^2}. \quad (\text{A13})$$

Combining Eqs. (A7), (A8), and (A13) we find

$$\begin{aligned} \theta_1^>(\mathbf{k}, t) &\approx \frac{g}{\lambda} \int d^2r \exp[-i\mathbf{k} \cdot \mathbf{r}] \sin[\theta^<(\mathbf{r}, t)] \\ & - \frac{g}{\lambda\omega_\Lambda^2} \int d^2r \exp[-i\mathbf{k} \cdot \mathbf{r}] \cos[\theta^<(\mathbf{r}, t)] \ddot{\theta}^<(\mathbf{r}, t), \end{aligned} \quad (\text{A14})$$

where we used  $\Lambda a = 1$  again. Here we neglected by the term proportional to  $[\theta^<(\mathbf{r}, t)]^2$  because it leads to a subdominant (in the RG sense) contribution. From this we find that

$$\begin{aligned} \theta_1^>(\mathbf{r}, t) &\approx \frac{g}{\lambda} \int_{\text{shell}} \frac{d^2k}{(2\pi)^2} e^{i\mathbf{k} \cdot \mathbf{r}} \int d^2x e^{-i\mathbf{k} \cdot \mathbf{x}} \sin[\theta^<(\mathbf{x}, t)] - \frac{g}{\lambda^2 \Lambda^2 \mu} \\ & \times \int_{\text{shell}} \frac{d^2k}{(2\pi)^2} e^{i\mathbf{k} \cdot \mathbf{r}} \int d^2x e^{-i\mathbf{k} \cdot \mathbf{x}} \cos[\theta^<(\mathbf{x}, t)] \ddot{\theta}^<(\mathbf{x}, t). \end{aligned} \quad (\text{A15})$$

We now consider the term  $(g/a^2) \cos[\theta^<(\mathbf{r}, t)] \theta_1^>(\mathbf{r}, t)$

$$\begin{aligned} & \frac{g}{a^2} \cos[\theta^<(\mathbf{r}, t)] \theta_1^>(\mathbf{r}, t) \\ & \approx \frac{g^2}{\lambda a^2} \int_{\text{shell}} \frac{d^2k}{(2\pi)^2} e^{i\mathbf{k} \cdot \mathbf{r}} \int d^2x e^{-i\mathbf{k} \cdot \mathbf{x}} \frac{1}{2} \sin[\theta^<(\mathbf{x}, t) - \theta^<(\mathbf{r}, t)] \\ & - \frac{g^2}{\lambda^2 \mu} \int_{\text{shell}} \frac{d^2k}{(2\pi)^2} e^{i\mathbf{k} \cdot \mathbf{r}} \int d^2x e^{-i\mathbf{k} \cdot \mathbf{x}} \frac{1}{2} \ddot{\theta}^<(\mathbf{x}, t), \end{aligned} \quad (\text{A16})$$

where we neglected terms such as  $\sin[2\theta^<(\mathbf{r}, t)]$ . Because we are integrating over the high-momentum shell this integral will be suppressed unless  $\mathbf{x}$  is close to  $\mathbf{r}$ . This suggests a change of variables  $\mathbf{x} = \mathbf{r} + \xi$  and Taylor expanding  $\theta^<(\mathbf{x}, t)$  in powers of  $\theta^<(\mathbf{x}, t) \approx \theta^<(\mathbf{r}, t) + \theta^<(\mathbf{r}, t) + \frac{1}{2} \xi_\alpha \xi_\beta \frac{\partial^2 \theta^<(\mathbf{r}, t)}{\partial r_\alpha \partial r_\beta}$ . Then

$$\frac{g}{a^2} \cos[\theta^<(\mathbf{r}, t)] \theta_1^>(\mathbf{r}, t) \approx \frac{C_2}{8\pi} \frac{g^2}{\lambda} \frac{\delta\Lambda}{\Lambda} \Delta\theta - \frac{C_1}{4\pi} \frac{g^2}{\lambda^2 \mu} \frac{\delta\Lambda}{\Lambda} \ddot{\theta}, \quad (\text{A17})$$

where

$$\frac{C_1}{\Lambda^2} = \int d^2\xi J_0(\Lambda\xi), \quad \frac{C_2}{\Lambda^4} = \int d^2\xi \xi^2 J_0(\Lambda\xi). \quad (\text{A18})$$

When we need to substitute these expressions back into Eq. (A9), we find that the term containing  $\Delta\theta$  renormalizes the coupling  $\lambda$  as

$$\lambda \rightarrow \lambda + \frac{C_2}{8\pi} \frac{g^2}{\lambda} \frac{\delta\Lambda}{\Lambda}. \quad (\text{A19})$$

In addition there is an extra term proportional to  $\ddot{\theta}$  generated in Eq. (A9), which renormalizes  $\mu$

$$\frac{1}{\mu} \rightarrow \frac{1}{\mu} + \frac{C_1}{4\pi} \frac{g^2}{\lambda^2 \mu} \frac{\delta\Lambda}{\Lambda}. \quad (\text{A20})$$

Finally we restore the cutoff by rescaling  $\mathbf{k} \rightarrow \mathbf{k}(1 - \delta\Lambda/\Lambda)$ ,  $\mathbf{r} \rightarrow \mathbf{r}(1 + \delta\Lambda/\Lambda)$ ,  $t \rightarrow t(1 + \delta\Lambda/\Lambda)$ , and  $p \rightarrow p(1 - \delta\Lambda/\Lambda)$ . This rescaling additionally renormalizes the coupling  $g$ :  $g \rightarrow g(1 + 2\delta\Lambda/\Lambda)$ . Combining this result with Eqs. (A11), (A19), and (A20) we find the following renormalization group equations

$$\frac{dg}{dl} = g \left( 2 - \frac{1}{4\pi v_0} \frac{1}{K} \right), \quad (\text{A21})$$

$$\frac{dK}{dl} = \frac{1}{16\pi K} \frac{g^2}{v^2} (C_2 + 2C_1), \quad (\text{A22})$$

$$\frac{dv}{dl} = \frac{g^2}{16\pi v K^2} (C_2 - 2C_1), \quad (\text{A23})$$

where  $l = \ln \Lambda$ . We can read off from Eq. (A23) that if the system contains a fixed velocity, for example in relativistic systems, we need to have  $C_2 = 2C_1$  to enforce that the velocity is invariant under the flow.

Note that if the initial system is already close to the critical point then the RG equations above simplify to

$$\frac{dg}{dl} \approx g \left( 2 - \frac{1}{4\pi\lambda} \right), \quad (\text{A24})$$

$$\frac{d\lambda}{dl} \approx \frac{C_2}{8\pi} \frac{g^2}{\lambda}, \quad (\text{A25})$$



which are equivalent to Eqs. (40) and (41). Note that a more complete set of RG equations (A21)–(A23) have the same universal predictions of the dynamical phase transitions and exponential divergence of the time scales as the simplified equations above. Also note that the real RG equations bear close analogy to the flow equations in imaginary time characterizing the equilibrium Kosterlitz-Thouless transition [36]. Thus the nonequilibrium KT transition discussed here is characterized

by exponentially divergent length and time scales. Physically these long scales characterize a very slow process of vortex unbinding and equilibration at long distances. Note that the RG equations (A21)–(A23) also implicitly take into account renormalization of the temperature in the system. This comes from the fact that creating vortex-antivortex pairs removes the energy from the phonon degrees of freedom. We are going to investigate this issue in more detail in a separate publication.

- 
- [1] K. B. Davis, M.-O. Mewes, M. R. Andrews, N. J. van Druten, D. S. Durfee, D. M. Kurn, and W. Ketterle, *Phys. Rev. Lett.* **75**, 3969 (1995); M. H. Anderson, J. R. Ensher, M. R. Matthews, C. E. Wieman, and E. A. Cornell, *Science* **269**, 198 (1995); C. C. Bradley, C. A. Sackett, J. J. Tollett, and R. G. Hulet, *Phys. Rev. Lett.* **75**, 1687 (1995).
  - [2] M. Greiner *et al.*, *Nature (London)* **415**, 39 (2002).
  - [3] C. A. Regal, M. Greiner, and D. S. Jin, *Phys. Rev. Lett.* **92**, 040403 (2004); M. W. Zwierlein, C. A. Stan, C. H. Schunck, S. M. F. Raupach, A. J. Kerman, and W. Ketterle, *ibid.* **92**, 120403 (2004); M. Bartenstein, A. Altmeyer, S. Riedl, S. Jochim, C. Chin, J. H. Denschlag, and R. Grimm, *ibid.* **92**, 120401 (2004); T. Bourdel, L. Khaykovich, J. Cubizolles, J. Zhang, F. Chevy, M. Teichmann, L. Tarruell, S. J. J. M. F. Kokkelmans, and C. Salomon, *ibid.* **93**, 050401 (2004).
  - [4] J. M. Kosterlitz and D. J. Thouless, *J. Phys. C* **6**, 1181 (1973); V. S. Berezinskii, *Sov. Phys. JETP* **34**, 610 (1972).
  - [5] Z. Hadzibabic, P. Krüger, M. Cheneau, B. Battelier, and J. B. Dalibard, *Nature (London)* **441**, 1118 (2006).
  - [6] P. Clade, C. Ryu, A. Ramanathan, K. Helmerson, and W. D. Phillips, *Phys. Rev. Lett.* **102**, 170401 (2009).
  - [7] C. D. Fertig, K. M. O'Hara, J. H. Huckans, S. L. Rolston, W. D. Phillips, and J. V. Porto, *Phys. Rev. Lett.* **94**, 120403 (2005); T. Stöferle, H. Moritz, C. Schori, M. Köhl, and T. Esslinger, *ibid.* **92**, 130403 (2004).
  - [8] M. R. Matthews, B. P. Anderson, P. C. Haljan, D. S. Hall, C. E. Wieman, and E. A. Cornell, *Phys. Rev. Lett.* **83**, 2498 (1999); K. W. Madison, F. Chevy, W. Wohlleben, and J. Dalibard, *ibid.* **84**, 806 (2000); Z. Dutton, M. Budde, C. Slowe, and L. V. Hau, *Science* **293**, 663 (2001).
  - [9] S. Burger, K. Bongs, S. Dettmer, W. Ertmer, K. Sengstock, A. Sanpera, G. V. Shlyapnikov, and M. Lewenstein, *Phys. Rev. Lett.* **83**, 5198 (1999); B. P. Anderson, P. C. Haljan, C. A. Regal, D. L. Feder, L. A. Collins, C. W. Clark, and E. A. Cornell, *ibid.* **86**, 2926 (2001); J. Denschlag, J. E. Simsarian, D. L. Feder, C. W. Clark, L. A. Collins, J. Cubizolles, L. Deng, E. W. Hagley, K. Helmerson, W. P. Reinhardt, S. L. Rolston, B. I. Schneider, and W. D. Phillips, *Science* **287**, 97 (2000).
  - [10] T. Kinoshita, T. Wenger, and D. S. Weiss, *Nature (London)* **440**, 900 (2006).
  - [11] L. E. Sadler, J. M. Higbie, S. R. Leslie, M. Vengalattore, and D. M. Stamper-Kurn, *Nature (London)* **443**, 312 (2006).
  - [12] I. Bloch, J. Dalibard, and W. Zwerger, *Rev. Mod. Phys.* **80**, 885 (2008).
  - [13] C. Raman, M. Köhl, R. Onofrio, D. S. Durfee, C. E. Kuklewicz, Z. Hadzibabic, and W. Ketterle, *Phys. Rev. Lett.* **83** 2502 (1999).
  - [14] E. Altman and A. Auerbach, *Phys. Rev. Lett.* **89**, 250404 (2002); R. A. Barankov, L. S. Levitov, and B. Z. Spivak, *ibid.* **93**, 160401 (2004); P. Calabrese and J. Cardy, *ibid.* **96**, 136801 (2006); *J. Stat. Mech: Exp.* (2007) P06008; K. Sengupta, S. Powell, and S. Sachdev, *Phys. Rev. A* **69**, 053616 (2004); C. Kollath, A. M. Läuchli, and E. Altman, *Phys. Rev. Lett.* **98**, 180601 (2007); E. A. Yuzbashyan, B. L. Altshuler, V. B. Kuznetsov, and V. Z. Enolskii, *Phys. Rev. B* **72**, 220503(R) (2005); D. J. Reilly, J. M. Taylor, E. A. Laird, J. R. Petta, C. M. Marcus, M. P. Hanson, and A. C. Gossard, *Phys. Rev. Lett.* **101**, 236803 (2008); G. Roux, *Phys. Rev. A* **79**, 021608 (2009); V. Gritsev, E. Demler, M. D. Lukin, and A. Polkovnikov, *Phys. Rev. Lett.* **99**, 200404 (2007); S. R. Manmana, S. Wessel, R. M. Noack, and A. Muramatsu, *ibid.* **98**, 210405 (2007); A. Iucci and M. A. Cazalilla, e-print arXiv:0903.1205; P. Barmettler, M. Punk, V. Gritsev, E. Demler, and E. Altman, *Phys. Rev. Lett.* **102**, 130603 (2009).
  - [15] M. Rigol, V. Dunjko, and M. Olshanii, *Nature (London)* **452**, 854 (2008); P. Reimann, *Phys. Rev. Lett.* **101**, 190403 (2008); M. Rigol, *ibid.* **103**, 100403 (2009).
  - [16] A. Polkovnikov, *Phys. Rev. B* **72**, 161201(R) (2005); W. H. Zurek, U. Dorner, and P. Zoller, *Phys. Rev. Lett.* **95**, 105701 (2005); J. Dziarmaga, *ibid.* **95**, 245701 (2005); R. W. Cherng and L. S. Levitov, *Phys. Rev. A* **73**, 043614 (2006); A. Polkovnikov and V. Gritsev, *Nature Physics* **4**, 477 (2008); A. Altland and V. Gurarie, *Phys. Rev. Lett.* **100**, 063602 (2008); C. De Grandi, R. A. Barankov, and A. Polkovnikov, *ibid.* **101**, 230402 (2008); K. Sengupta, D. Sen, and S. Mondal, *ibid.* **100**, 077204 (2008); D. Sen, K. Sengupta, and S. Mondal, *ibid.* **101**, 016806 (2008); U. Divakaran, V. Mukherjee, A. Dutta, and D. Sen, *J. Stat. Mech.* (2009) P02007; D. Chowdhury, U. Divakaran, and A. Dutta, *Phys. Rev. E* **81**, 012101 (2010); K. Sengupta and D. Sen, *Phys. Rev. A* **80**, 032304 (2009); A. P. Itin and P. Törmä, e-print arXiv:0901.4778; D. Rossini, A. Silva, G. Mussardo, and G. E. Santoro, *Phys. Rev. Lett.* **102**, 127204 (2009); F. Pollmann, S. Mukherjee, A. G. Green, and J. E. Moore, e-print arXiv:0907.3206; K. Rodriguez, A. Argüelles, and L. Santos, e-print arXiv:0905.3312; A. Bermudez, D. Patane, L. Amico, M. A. Martin-Delgado, *Phys. Rev. Lett.* **102**, 135702 (2009).
  - [17] S. Hofferberth, I. Lesanovsky, B. Fischer, T. Schumm, and J. Schmiedmayer, *Nature (London)* **449**, 324 (2007).
  - [18] A. A. Burkov, M. D. Lukin, and E. Demler, *Phys. Rev. Lett.* **98**, 200404 (2007).
  - [19] R. Bistritzer and E. Altman, *PNAS* **104**, 9955 (2007).

- [20] I. E. Mazets and J. Schmiedmayer, e-print arXiv:0806.4431.
- [21] L. Mathey, A. Polkovnikov, and A. H. Castro Neto, EuroPhys. Lett. **81**, 10008 (2008).
- [22] M. A. Cazalilla, A. Iucci, and T. Giamarchi, Phys. Rev. A **75**, 051603(R) (2007).
- [23] T. W. B. Kibble, J. Phys. A **9**, 1387 (1976); Physics Today **60**, 47 (2007).
- [24] W. H. Zurek, Nature (London) **317**, 505 (1985).
- [25] L. Mathey and A. Polkovnikov, Phys. Rev. A **80**, 041601(R) (2009).
- [26] S. Sachdev, *Quantum Phase Transitions*, (Cambridge University Press, Cambridge, England, 1999).
- [27] P. B. Blakie, A. S. Bradley, M. J. Davis, R. J. Ballagh, and C. W. Gardiner, Adv. Phys. **57**, 363 (2008).
- [28] A. Polkovnikov, Phys. Rev. A **68**, 053604 (2003).
- [29] A. Polkovnikov, e-print arXiv:0905.3384.
- [30] A. Polkovnikov, E. Altman, and E. Demler, Proc. Natl. Acad. Sci. USA **103**, 6125 (2006).
- [31] E. H. Lieb and D. W. Robinson, Commun. Math. Phys. **28**, 251 (1972).
- [32] P. Calabrese and J. Cardy, Phys. Rev. Lett. **96**, 136801 (2006); J. Stat. Mech.: Theor. and Exp. (**2007**) P06008.
- [33] X.-G. Wen, *Quantum Field Theory of Many-Body Systems* (Oxford University Press, Oxford, 2004).
- [34] C. De Grandi, V. Gritsev, and A. Polkovnikov, Phys. Rev. B **81**, 012303 (2010).
- [35] L. D. Landau and E. M. Lifshitz, *Mechanics*, (Butterworth-Heinemann, Oxford, 1982).
- [36] T. Giamarchi, *Quantum Physics in One Dimension*, (Clarendon Press, Oxford, 2004).